

IONIC WIND CONTROL IN AC SINGLE MAGNETIC PLASMA ACTUATOR BY MAGNETIC FIELD

T. Ueno¹, Y. Asaka¹, T. Kuwahara^{1,2}

¹ Department of Mechanical Systems Engineering, Graduate School of Nippon Institute of Technology,

4-1 Gakuendai, Miyashiromachi, Minamisaitama-gun, 3458501, Japan.

² Department of Mechanical Engineering, Nippon Institute of Technology,

4-1 Gakuendai, Miyashiromachi, Minamisaitama-gun, 3458501, Japan.

An AC single plasma actuator has been developed using a magnetic fluid (MF) and a dielectric barrier discharge (DBD), termed “single MF-DBD plasma actuator”. In this system, the DBD induces an ionic wind from the MF, which is held in place by an external magnetic field. This study investigates the effect of an external magnetic field on the ionic wind velocity. The experimental results indicated that the external magnetic field effectively controls the ionic wind velocity due to the interaction between the MF and the exposed electrode. The efficiency of the ionic wind generation is also analyzed and clarified.

Introduction.

Dielectric barrier discharges (DBDs) are extensively used in plasma actuators, ozone generators, and reactors. Due to their simple design, DBD plasma actuators can produce ionic wind, making them suitable for airflow control around an airfoil [1] and ozone generation [2]. Typically, the ionic wind velocity of a DBD plasma actuator is controlled by adjusting the input voltage. For a range of DBD plasma actuators, we introduced a novel DBD plasma actuator equipped with a magnetic fluid (MF) [3], referred to as an MF-DBD plasma actuator. The ionic wind velocity of the MF-DBD plasma actuator is influenced by the size of the MF overlapping the insulated electrode [4]. In addition to voltage control, the MF-DBD plasma actuator can regulate the ionic wind velocity using a magnetic field. In the context of applying an electric field to MF, previous research has explored the dielectric constant of MF under the influence of an electric field [5].

In this study, we investigate how magnetic fields can control the ionic wind velocity by examining the characteristics of the ionic wind velocity as a function of the overlapping distance between the MF and the exposed electrode under various magnetic field conditions. The overlapping distances between the exposed and insulated electrodes at various magnetic flux densities are presented. The discharge power is determined using the Q - V Lissajous technique [6]. The efficiency of the ionic wind generation is then calculated based on the measured ionic wind velocity U and discharge power P_{QV} .

1. Working principle of the MF-DBD plasma actuator. Fig. 1 illustrates a schematic of the single MF-DBD plasma actuator. The principle of ionic wind generation in the MF-DBD plasma actuator is similar to that of conventional DBD plasma actuators, as explained by E. Moreau, *et al.* [7]. Based on their research, nonthermal plasma (NTP) is generated when a high AC voltage is applied to the DBD plasma actuators. A streamer discharge occurs when a positive voltage is applied, whereas glow discharge occurs when a negative voltage is applied. The rapid repetition of these two discharges generates an ionic wind.

Glow discharge is more effective than streamer discharge for generating ionic wind.

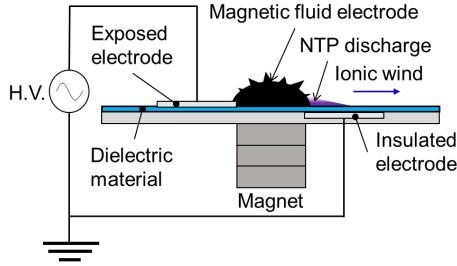


Fig. 1. Schematic diagram of the single MF-DBD plasma actuator.

The principle of the MF-DBD plasma actuator is explained as follows [3]: When a high AC voltage is applied to the MF-DBD plasma actuator, dielectric breakdown of the air occurs, followed by nonthermal plasma generation. The MF electrode on the dielectric periodically changes polarity. When the MF electrode is negative, electrons are emitted from the MF electrode towards the insulated electrode. At this time, positive ions are generated, which contribute to the generation of ionic wind. Then, electrons are accumulated on the dielectric. When the MF electrode is positive, a large number of electrons accumulated on the dielectric move towards the MF electrode. In this case, the total amount of the electron is larger than when the MF electrode is negative. On the contrary, the generated positive ions move in the opposite direction to the electrons. As the electrons move to the electrode in a very short time due to their high mobility, the positive ions remain. These drifting positive ions collide with neutral particles. This collision induces the ionic wind.

2. Experimental setup and method.

Fig. 2 shows an MF-DBD plasma actuator with its dimensions. The MF-DBD plasma actuator comprises acrylic, glass, aluminum tape, neodymium magnets, and water-based MF (W-40, Ichinen Chemicals Co., Ltd.). Aluminum tape is used as the electrode, and the exposed electrode is in direct contact with the MF. The magnetic flux density B required to stabilize the MF is $B_c = 86.6 \times 10^{-4} \text{ T}$ [8]. A surface DBD is

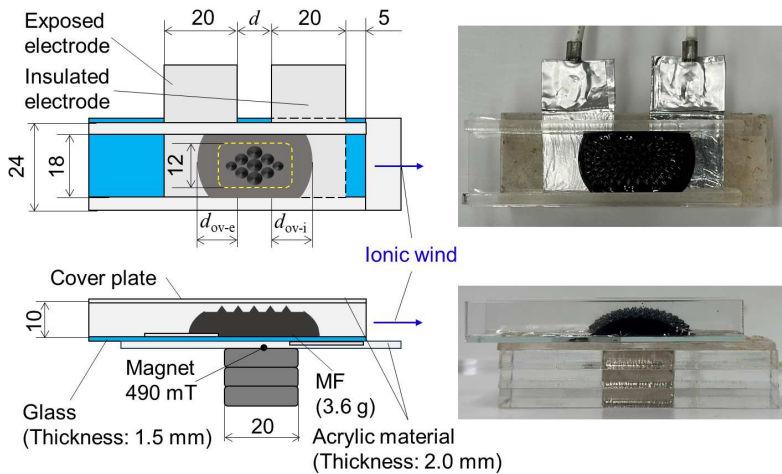


Fig. 2. Single MF-DBD plasma actuator with dimensions.

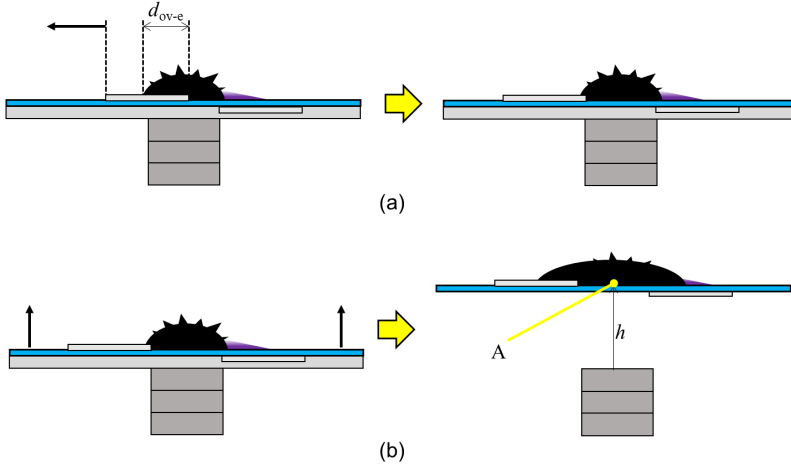


Fig. 3. Two experimental methods for ionic wind velocity measurement. (a) Only the overlapping distance of the exposed electrode d_{ov-e} is varied. (b) Magnetic flux density B is varied using magnets.

generated at the edge of the MF when a high AC voltage is applied to the aluminum tape, and ionic wind is excited.

Fig. 3 shows an explanatory diagram of the experimental method. Two separate experiments are conducted. The first experiment aims to investigate the relationship between the ionic wind velocity U and the overlapping distance of the exposed electrode d_{ov-e} . The second experiment focuses on examining the effect of the magnetic field on the ionic wind velocity U . As shown in Fig. 3a, the overlapping distance of the insulated electrodes d_{ov-i} is fixed at 13 mm, while the distance between the electrodes d is increased. The range of the distance between the electrodes is $d = 10-20$ mm. In Fig. 3(b), the magnetic flux density B applied to the MF is adjusted by sequentially inserting 2 mm acrylic plates. The distance between the electrodes d is fixed at $d = 18$ mm. The magnetic flux density B is measured at point A as the acrylic height is varied. A tesla meter (MT-801, Mother Toll Co., Ltd.) is employed for these measurements. Fig. 4 illustrates the experimental setup for the single MF-DBD plasma actuator and its electrical connections during the measurements. A high AC voltage power supply (LHV-13AC, Logy Electric Co., Ltd.) that can generate a discharge voltage of 10 kV at a frequency of 9 kHz is used to apply a high alternating voltage to the electrodes. A hot-wire anemometer (AM-4224SD, Mother Tool Co., Ltd.) is used to measure the ionic wind velocity U . The ionic wind velocity U is measured 10 mm from the edge of the insulated electrode. The capacitor is removed during the ionic wind experiment. The ionic wind velocity U is measured six times, and the mean and standard error are computed for each set of measurements. The discharge power P_{QV} is determined using the $Q-V$ Lissajous approach, which is applied to the MF-DBD plasma actuator. As illustrated in Fig. 4, a capacitor is installed to measure the discharge voltage V and the electric charge in the capacitor C . The Lissajous figure is generated after the measurements. The discharge power P_{QV} is then calculated as the product of the area of the figure and the discharge frequency f . The electric charge in the capacitor C is calculated by multiplying the differential voltage V_d by the capacitance of the capacitor c . An oscilloscope (SDS6062, Owon Technology Inc.), high-voltage probe (P6015A, Tektronix Inc.), and differential probe (DP10013,

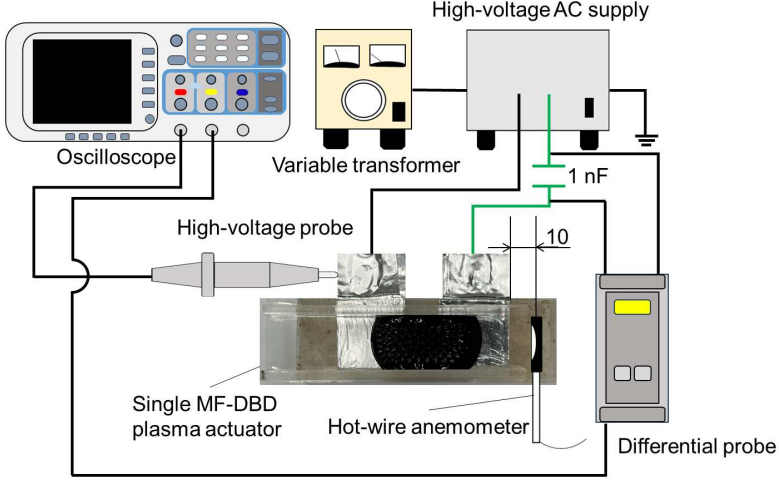


Fig. 4. Experimental setup and measurements.

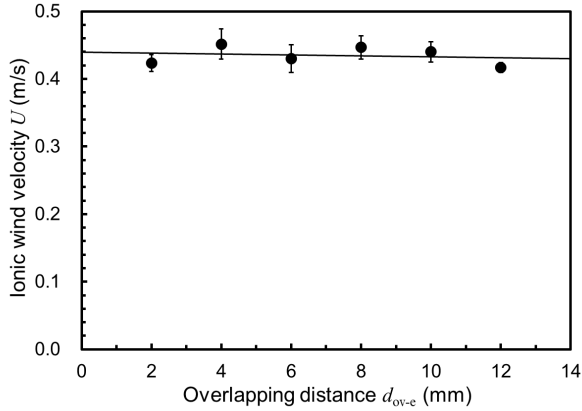


Fig. 5. Experimental results of the overlapping distance of the exposed electrode d_{ov-e} and ionic wind velocity U .

Shenzhen Micsing Technology Co., Ltd.) are used to measure the discharge voltage V and differential voltage V_d . The capacitance of the capacitor c is 1 nF. The data obtained from the oscilloscope is $760 \mu\text{s}$, and the obtained data are filtered using the least squares method [9]. The ionic wind generation energy efficiency η_U is calculated from the measured ionic wind velocity U and discharge power P_{QV} as follows:

$$\eta_U = \frac{U}{P_{QV}}. \quad (1)$$

3. Experimental results and discussion.

Fig. 5 shows the relationship between the overlapping distance of the exposed electrode d_{ov-e} and the ionic wind velocity U . The experimental results indicate that the ionic wind velocity U is constant, regardless of variations in the overlapping distance of the exposed electrode d_{ov-e} . Based on these findings and the characteristics of the ionic

wind velocity described in [4], the ionic wind velocity of the MF-DBD plasma actuator depends only on the overlapping distance of the insulated electrode d_{ov-i} . It appears that the current from the exposed electrode into the MF electrode is constant even if the overlapping distance of the exposed electrode d_{ov-e} is varied. The ionic wind velocity U is proportional to the square root of the current I as follows:

$$U \propto \sqrt{I}. \quad (2)$$

Therefore, the ionic wind velocity is independent of the overlapping distance of the exposed electrode d_{ov-e} .

Fig. 6a illustrates the relationship between the magnetic flux density B and the overlapping distance d_{ov} of each electrode. When the initial magnetic flux density is set as $B = 305$ mT, the overlapping distance d_{ov} of each electrode are $d_{ov-i} = 5$ mm and $d_{ov-e} = 12$ mm. The d_{ov} is measured as B decreases. It is noted that d_{ov} is constant for B above 161 mT. The MF is held on the device by the magnetic body force generated inside the MF. The magnetic body force \mathbf{F} is given by the following equation:

$$\mathbf{F} = \mathbf{M} \cdot \nabla \mathbf{H}, \quad (3)$$

where \mathbf{M} is the magnetization of the MF, and \mathbf{H} is the magnetic field. To simplify the discussion, a one-dimensional analysis is employed. The magnetic body force is replaced by

$$F = M \frac{dH}{dh} = \mu_0 \chi_m H \frac{dH}{dh}, \quad (4)$$

where h is height from magnet to MF, μ_0 is vacuum permeability, χ_m is magnetic susceptibility. In other words, the overlapping distance d_{ov} of each electrode depends on this force \mathbf{F} , that is, the gradient of H or B . Therefore, the magnetic body force \mathbf{F} can be expressed as follows:

$$F = f_1 \left(\frac{HdH}{dh} \right), F = f_2 \left(\frac{BdB}{dh} \right), B = \mu_0 H, \quad (5)$$

where f_i stands for a function with $i = 1-7$. In the MF-DBD plasma actuator, d_{ov} tends to increase as an increase of the distance between the MF and the magnet surface. That is, d_{ov} is a function of $1/F$ as follows:

$$d_{ov} = f_3 \left(\frac{1}{F} \right) = f_4 \left(\frac{dh}{BdB} \right). \quad (6)$$

In this study, $dh = 2$ mm. It is noted that d_{ov} in the formulas is in m, whereas measured d_{ov} is in mm. Thus, Eq. (6) is replaced by

$$d_{ov} = f_5 \left(\frac{1}{B^2} \right). \quad (7)$$

Fig. 6b illustrates the relationship between the magnetic flux density gradient dB/dh and the overlapping distance d_{ov} of each electrode. Here, Eq. (6) is formulated as follows:

$$d_{ov} = f_4 \left(\frac{dh}{BdB} \right) = f_6 \left\{ \left(\frac{dh}{dB} \right)^2 \frac{dB}{Bdh} \right\}. \quad (8)$$

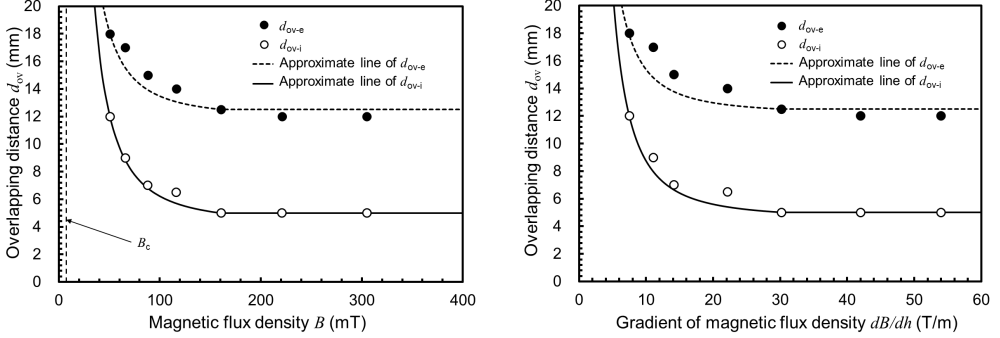


Fig. 6. Relationship between magnetic field and the overlapping distance of each electrode. (a) Relationship between the magnetic flux density B and the overlapping distance d_{ov} . (b) Relationship between the gradient of the magnetic flux density dB/dh and the overlapping distance d_{ov} .

Table 1. Resulting m and n parameters obtained from the experiments in Figs. 6a,b.

	(a)	(b)
d_{ov-i}	$m_1 : 2.0 \times 10^{-2} \text{ T}^2, n_1 : 4.2 \times 10^{-3} \text{ m}$	$m_3 : 4.2 \times 10^2 \text{ T}^2/\text{m}, n_3 : 4.5 \times 10^{-3} \text{ m}$
d_{ov-e}	$m_2 : 1.6 \times 10^{-2} \text{ T}^2, n_2 : 1.2 \times 10^{-2} \text{ m}$	$m_4 : 3.3 \times 10^2 \text{ T}^2/\text{m}, n_4 : 1.2 \times 10^{-2} \text{ m}$

It is noted that dB/B can be considered constant in the range of $h = 3.5 - 15.5$ mm, which is performed in this investigation. In this case, d_{ov} is given by

$$d_{ov} \cong f_7 \left\{ \left(\frac{dh}{dB} \right)^2 \right\}. \quad (9)$$

Fig. 6 illustrates that a larger overlapping distance of each electrode is achieved in a magnetic field with a lower magnetic flux density B . This relationship can be expressed as follows, with constants m and n presented in Table 1 for Figs. 6a,b:

$$d_{ov-i} = m_1 \frac{1}{B^2} + n_1, \quad d_{ov-e} = m_2 \frac{1}{B^2} + n_2, \quad (10)$$

$$d_{ov-i} = m_3 \frac{1}{(dB/dh)^2} + n_3, \quad d_{ov-e} = m_4 \frac{1}{(dB/dh)^2} + n_4. \quad (11)$$

Fig. 7 shows the discharge photographs captured when the magnetic flux density B and the overlapping distance of the insulated electrode d_{ov-i} are varied. Observations from these photographs in Fig. 7 indicate that a shorter overlapping distance of the insulated electrode d_{ov-i} tends to produce longer streamers. However, these streamers have a minimal impact on ionic wind generation [7]. In addition, a trade-off exists between the streamers and the glow discharge in the DBD. The DBD contains a large amount of glow discharge as the overlapping distance of the insulated electrode d_{ov-i} increases. Based on this observation, we infer that the ionic wind velocity U increases as the overlapping distance of the insulated electrode d_{ov-i} increases.

Fig. 8a shows the relationship between the ionic wind velocity U and the overlapping distance of the insulated electrode d_{ov-i} . Fig. 8(b) illustrates the relationship between

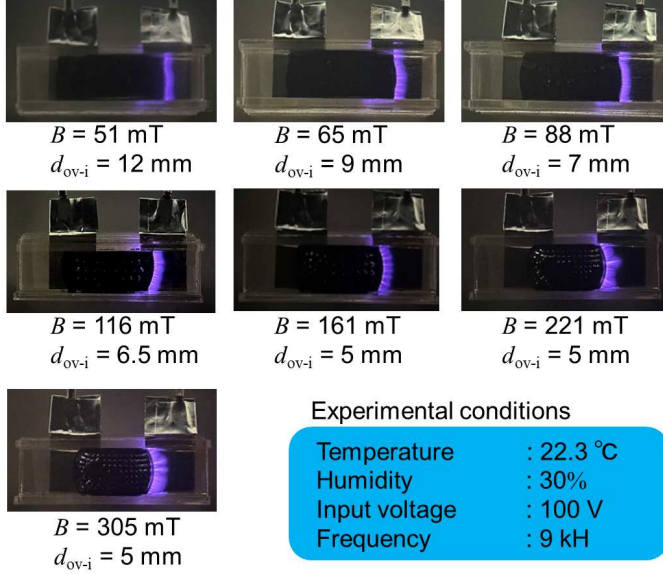


Fig. 7. Top-view photographs of the NTP discharge at different magnetic flux densities B .

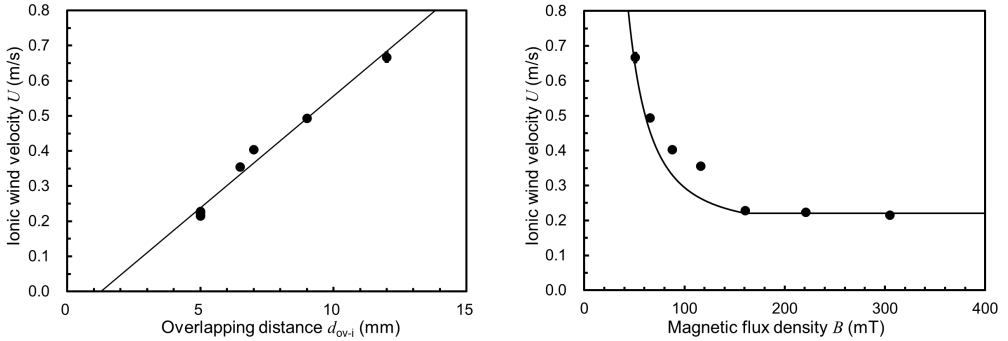


Fig. 8. Relationship between magnetic field and ionic wind. (a) Relationship between the ionic wind velocity U and the overlapping distance of the insulated electrode d_{ov-i} . (b) Relationship between magnetic flux density B and ionic wind velocity U .

the ionic wind velocity U and the magnetic flux density B . The measurement results indicate that the ionic wind velocity U increases as the magnetic flux density B decreases due to the corresponding increase in the overlapping distance of the insulated electrodes d_{ov-i} . The ionic wind velocity U in Fig. 8a is approximated by

$$U = k_1 d_{ov-i} + U_1, \quad (12)$$

where $k_1 = 63.7 \text{ s}$, $U_1 = -0.08 \text{ m/s}$. Substitution of Eq. (10) into Eq. (12) yields the following approximate expression:

$$U = k_1 \left(m \frac{1}{B^2} + n \right) + U_1. \quad (13)$$

These results indicate that the MF-DBD plasma actuator can control the ionic wind velocity U by controlling the magnetic field.

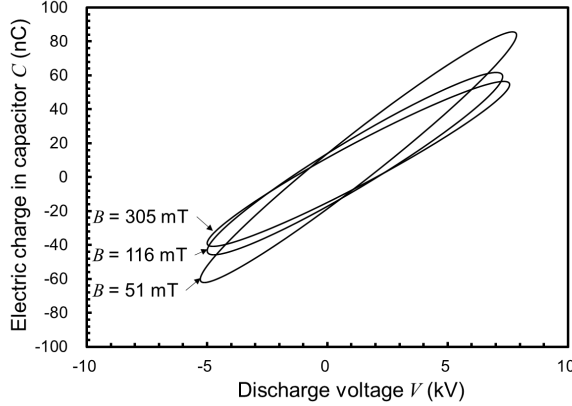


Fig. 9. Q - V Lissajous figures at different magnetic flux density B .

Fig. 9 illustrates the Q - V Lissajous figures for the magnetic flux densities $B = 51$ mT, $B = 116$ mT, and $B = 305$ mT. In the Q - V Lissajous figure analysis, a parallelogram Q - V Lissajous figure indicates that discharge, and non-discharge are clearly occurring in one DBD cycle, whereas an elliptical Q - V Lissajous figure indicates that continuous discharge occurs in one DBD cycle. The resulting elliptical figures in Fig. 9 indicate that continuous discharge occurs in one DBD cycle and that the generated ions are trapped in the discharge space. These Lissajous figures show that the electric charge in the capacitor C and discharge power P_{QV} increase as the magnetic flux density B decreases. Furthermore, the discharge voltage V does not significantly change with the magnetic flux density B .

Fig. 10 illustrates the calculated ionic wind energy generation efficiency η_U . The efficiency hU can be expressed as follows:

$$\eta_U = k_2 B^\alpha, \quad (14)$$

where $k_2 = 1.8 \text{ m}/(\text{J}\cdot\text{mT})$, $\alpha = -0.7$. Eq. (14) indicates that a decrease in magnetic flux density B leads to an increase in the ionic wind generation efficiency η_U .

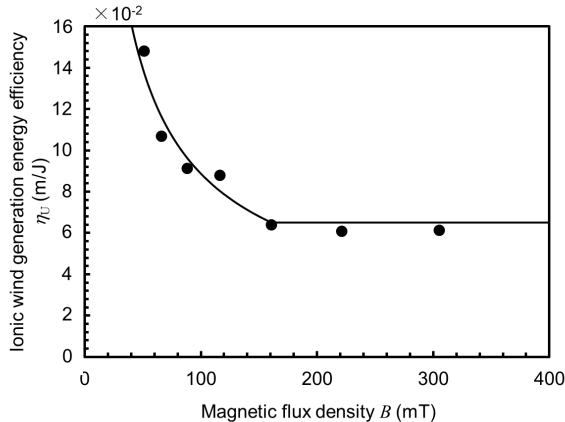


Fig. 10. Relationship between ionic wind generation efficiency η_U and magnetic flux density B .

4. Conclusions

In this study, to demonstrate that magnetic fields can control the ionic wind velocity, the characteristics of the ionic wind velocity are examined under different magnetic fields. The following conclusions are obtained:

- When only the overlapping distance of the exposed electrodes d_{ov-e} is adjusted, the ionic wind velocity U is constant. Based on these observations and previous findings, the ionic wind velocity U generated by the MF-DBD plasma actuator depends only on the overlapping distance of the insulated electrodes d_{ov-i} .
- As the magnetic flux density B decreases, the overlapping distance d_{ov} between each electrode increases. Experimental results clearly show that d_{ov} is a function of the inverse of F , which is the magnetic body acting on the magnetic fluid, as well as $1/B^2$.
- Experimental observations of the DBD discharges indicate that as the overlapping distance of the insulated electrode d_{ov-i} increases, the DBD exhibits a large amount of glow discharge, which enhances ionic wind generation.
- This study demonstrates that a magnetic field can control the ionic wind velocity U of an MF-DBD plasma actuator. The characteristics of U are also revealed.
- The Q - V Lissajous method shows that a lower magnetic flux density B results in a higher discharge power P_{QV} . Furthermore, an analysis of the ionic wind generation energy efficiency η_U based on discharge power P_{QV} and ionic wind velocity U indicates that a decrease in magnetic flux density B improves the efficiency η_U .

References

- [1] P.A. POLIVANOV, A.A. SIDORENKO AND A.A. MASLOV. Effective plasma buffet and drag control for laminar transonic aerofoil. *Proc. Inst. Mech. Eng., Part G: J. Aerosp. Eng.*, vol. 234 (2018), no. 1.
- [2] M. BELAN AND F. MESSANELLI. Compared ionic wind measurements on multi-tip corona and DBD plasma actuators. *J. Electrostat.*, vol. 76 (2015), pp. 278–287.
- [3] T. KUWAHARA AND Y. ASAKA. Fundamental characteristics of single dielectric barrier discharge plasma actuator using magnetic fluid. *Int. J. Plasma Environ. Sci. Technol.*, vol. 17 (2023), e02001.
- [4] T. KUWAHARA AND Y. ASAKA. Ionic wind and ozone generation in a single magnetic fluid dielectric barrier discharge plasma actuator with different electrode configurations. *J. Magn. Magn. Mat.*, vol. 589 (2024), 171572.
- [5] M. RAJNAK, *et al.* Dielectric properties of magnetic fluids based on transformer oil ito 100 in a high frequency electric field. *Magnetohydrodynamics*, vol. 49 (2013), no. 3–4, pp. 265–269
- [6] H. JIANG, *et al.* Experimental Study of Q - V Lissajous Figures in Nanosecond-Pulse Surface Discharge. *IEEE Trans. Dielectr. Electr. Insul.*, vol. 20 (2013), no. 4, pp. 1101–1111.
- [7] E. MOREAU AND N. BENARD. Ionic wind produced by volume corona discharges and surface dielectric barrier discharges: What role do streamers play?. *J. Electrostat.*, vol. 132 (2024), 103988.
- [8] Y. FUKUDA AND N. DOUHARA. Study on interfacial phenomena of magnetic fluids. *JSME Int. J. Ser. B Fluids Therm. Eng.*, vol. 48 (2005), pp. 735–742.

- [9] J. KRIEGSEIS, *et al.* Capacitance and power consumption quantification of dielectric barrier discharge(DBD) plasma actuators. In *J. Electrostat.*, vol. 69 (2011), pp. 302–312.

Received 24.11.2024